Capturing Size and Intensity Changes of Hurricanes Irma and Maria (2017) from Polar-Orbiting Satellite Microwave Radiometers

XIAOXU TIAN AND XIAOLEI ZOU

*Cooperative Institute for Climate and Satellites, Earth Science System Interdisciplinary Center,
University of Maryland, College Park, College Park, Maryland*

ABSTRACT

A recently refined hurricane warm-core retrieval algorithm was applied to data from multiple polar-orbiting satellites that carry the Advanced Technology Microwave Sounder (ATMS) and the Advanced Microwave Sounding Unit-A (AMSU-A) to examine the diurnal variability of the warm cores of Hurricanes Irma and Maria. These hurricanes occurred during the 2017 hyperactive Atlantic hurricane season. Compared with data gathered by dropsondes within 100–1700 km of Hurricanes Irma and Harvey, the means and standard deviations of the differences between ATMS-derived and dropsonde-measured temperature profiles were less than 0.7 and 1 K, respectively, in the vertical layer between ~180 and 750 hPa. The temporal evolutions of the ATMS-derived and AMSU-A-derived maximum warm-core temperature anomalies followed more closely that of the minimum mean sea level pressure and slightly less closely that of the maximum sustained wind. The radii of the ATMS-derived warm cores at 4 and 6 K compared favorably with the 34- and 50-kt-wind radii, respectively, of Hurricane Irma (1 kt = 0.51 m s^{-1}). The vertical extent of the warm core toward lower levels increased with increasing intensity when Hurricane Irma experienced a strong intensification because of an enhanced latent heat release associated with diabatic processes. The tropical cyclone (TC) inner cores at upper-tropospheric levels (~250 hPa) were characterized by a single-peaked diurnal cycle with a maximum around midnight. This warm-core cycle may be an important element of TC dynamics and may have relevance to TC structural and intensity changes.

1. Introduction

Microwave temperature-sounding instruments such as the Advanced Microwave Sounding Unit-A (AMSU-A) on board the National Oceanic and Atmospheric Administration (NOAA) satellites *NOAA-15*, *-18*, and *-19*, the AMSU-A on board the European Organisation for the Exploitation of Meteorological Satellites (EUMETSAT) Meteorological Operational (MetOp) satellites *MetOp-A* and *-B*, and the Advanced Technology Microwave Sounder (ATMS) on board the NOAA *Suomi National Polar-Orbiting Partnership* (*SNPP*) satellite provide global measurements in the microwave part of the electromagnetic spectrum. There are 12 AMSU-A and 13 ATMS temperature-sounding channels located in the oxygen absorption band with central frequencies varying from 50.3 to 57.6 GHz. This makes the probing of

atmospheric temperatures in the vertical in almost all areas of tropical cyclones (TCs) without heavy precipitation possible.

The weighting functions of these AMSU-A and ATMS sounding channels are evenly distributed in the vertical from the surface up to ~0.1 hPa. This means that brightness temperatures measured in different channels are weighted functions of the atmospheric temperature within different atmospheric layers. The largest contribution of atmospheric radiation to a channel comes from the altitude where the weighting function of the channel peaks. Based on this physical consideration and since the launch of the first AMSU-A on board the *NOAA-15* satellite on 13 May 1998, several linear regression atmospheric temperature retrieval algorithms have been developed to derive three-dimensional atmospheric temperature fields in TCs (Kidder et al. 2000; Zhu et al. 2002; Brueske and Velden 2003; Demuth et al. 2004; Knaff et al. 2004; Demuth et al. 2006; Zhu and Weng 2013; Tian and Zou 2016). Using AMSU data for TC intensity and size estimations and for improving hurricane forecasts was documented in these previous studies

(e.g., Zhu et al. 2002; Demuth et al. 2004; Knaff et al. 2004; Demuth et al. 2006; Zhu and Weng 2013; Tian and Zou 2016). However, only some warm-core-related size and intensity parameters from a single AMSU-A instrument at a few instantaneous times were presented. Warm-core retrieval algorithms have also gone through a series of improvements over the past two decades.

The warm-core structure of TCs was examined in idealized simulations (Stern and Nolan 2012) and real-case simulations (Chen and Zhang 2013) using the Weather Research and Forecasting (WRF) Model. Specifically, the WRF Model, version 3.1.1, with a triply nested grid (e.g., 18-, 6-, and 2-km horizontal resolutions) and 40 vertical levels with the model top at 50 hPa (~20 km) was used by Stern and Nolan (2012) to simulate the development and maintenance of idealized intense hurricanes from a TC-like Rankine vortex on a doubly periodic f plane ($f = 5.031025\,\mathrm{s}^{-1}$) within a constant easterly environmental flow ($5\,\mathrm{m\,s}^{-1}$), and above a sea surface with a homogeneous and fixed temperature (28°C). They reported that the primary warm-core maximum temperature anomaly in idealized simulations occurred in the midtroposphere around 5–6 km and that a secondary weaker maximum temperature anomaly often appeared near 13–14 km. Through a series of model sensitivity experiments, they concluded that changes in the height of the warm core did not imply changes in either the intensity of the storm or the manner in which the winds in the eyewall decayed with height. In comparison, Durden (2013) examined the heights of eye thermal anomalies and found that the maximum temperature anomalies can vary between 760 and 250 hPa and suggested that model simulations should also exhibit such features. However, one limitation of the work is the small number of soundings extending to the upper levels of TC eyes. Chen and Zhang (2013) employed a quadruply nested grid (27-, 9-, 3-, and 1-km horizontal resolutions) and a cloud-permitting WRF Model with a model top at 30 hPa (~24 km) to make 72-h cloud-permitting predictions of Hurricane Wilma (2005). The 30-h model forecast produced a maximum warm core near the 13–15-km layer during Hurricane Wilma's rapid intensification. The 54-h model forecast produced a maximum warm core near the 11–13-km layer after the rapid intensification. Both maximum warm cores were located in the same layer as the upper-level outflow. It was argued that the upper-level warm core formed from an adiabatic warming of the subsidence of stratospheric air associated with the detrainment of convective bursts, while the upper-level divergent outflow tended to protect the warm core from ventilation by environmental flows and also prevented the accumulation of warm air in the eye by ventilating it into the environment.

In this study, an improved warm-core retrieval algorithm is applied to the four NOAA AMSU-A instruments on board the *NOAA-15*, *NOAA-18*, *NOAA-19*, and *SNPP* satellites during the lifetime of Hurricane Irma (2017) and to the four NOAA AMSU-A/ATMS instruments and the AMSU-A instrument on board the EUMETSAT *MetOp-B* satellite during the lifetimes of Hurricanes Irma, Maria and Harvey (2017). The five polar-orbiting operational satellite microwave instruments can provide observations of hurricanes at 2- or 3-h intervals. This allows the diurnal cycles of the TC warm-core structure and intensity to be captured. AMSU-A measurements from *MetOp-A* and -*B* for Hurricane Irma were not made available at the NOAA Comprehensive Large Array-data Stewardship System for reasons yet to be determined. In this study, we derive 8- or 10-times-daily three-dimensional atmospheric temperature fields during the entire lifetimes of Hurricanes Irma and Maria from brightness temperature measurements made by AMSU-A or ATMS on board the *NOAA-15*, *NOAA-18*, *NOAA-19*, *MetOp-B*, and *SNPP* satellites.

The paper is organized as follows. AMSU-A and ATMS data characteristics are briefly described in section 2. A quick review of temperature profile retrievals from brightness temperature observations made in the AMSU-A and ATMS temperature-sounding channels is provided in section 3. Results for Hurricanes Harvey and Irma are presented in section 4. Section 5 shows the structural evolution of Hurricane Maria at intervals of 2–3 h. The study is summarized and conclusions are given in section 6.

2. ATMS and AMSU-A data description

The ATMS is an advanced cross-track passive microwave radiometer on board the *SNPP* satellite. It has a total of 22 channels (Table 1). Channels 3–16 are temperature-sounding channels used to obtain vertical profiles of atmospheric temperature. Channels 1–2 and 16 are window channels that are sensitive to surface conditions and are not used for temperature profile retrievals. Since channels 3 and 4 are also sensitive to the surface, only channels 5–15 are used for atmospheric temperature retrievals in this study. The peak weighting functions for channels 5–15 at nadir are around 850, 700, 400, 250, 200, 100, 50, 25, 10, 5, and 2 hPa. Channels 17–22 are humidity-sounding channels and are not considered in this study. The ascending node of the ATMS on board the *SNPP* satellite crosses the equator at 1330 local time (LT), which is called the local equator crossing time (LECT). The swath width of the ATMS

TABLE 1. ATMS channel characteristics.

Channel	Frequency (GHz)	NEDT (K)	Beamwidth (°)	Peak weighting function (hPa)
1	23.8	0.5	5.2	Surface
2	31.4	0.6	5.2	Surface
3	50.3	0.7	2.2	Surface
4	51.76	0.5	2.2	950
5	52.8	0.5	2.2	850
6	53.596 ± 0.115	0.5	2.2	700
7	54.4	0.5	2.2	400
8	54.94	0.5	2.2	250
9	55.5	0.5	2.2	200
10	57.29	0.75	2.2	100
11	57.29 ± 0.217	1	2.2	50
12	57.29 ± 0.322 ± 0.048	1	2.2	25
13	57.29 ± 0.322 ± 0.022	1.25	2.2	10
14	57.29 ± 0.322 ± 0.010	2.2	2.2	5
15	57.29 ± 0.322 ± 0.0045	3.6	2.2	2
16	88.2	0.3	2.2	Surface
17	165.5	0.6	1.1	Surface
18	183.31 ± 7.0	0.8	1.1	800
19	183.31 ± 4.5	0.8	1.1	700
20	183.31 ± 3.0	0.8	1.1	500
21	183.31 ± 1.8	0.8	1.1	400
22	183.31 ± 1.0	0.9	1.1	300

scan is 2300 km, leaving almost no gaps between neighboring swaths so that near-full data coverage over the globe is achieved.

AMSU-A instruments are currently on board the *NOAA-19*, *-15*, and *-18* satellites, which have LECTs at 1530, 0621, and 0715 LT, respectively. The AMSU-A has a total of 15 channels. AMSU-A channels 4–14 are similar to ATMS channels 5–15. The AMSU-A has narrower scan swaths and larger gaps between two consecutive orbital swaths than the ATMS. AMSU-A temperature-sounding channels have a longer integration time and lower data noise than those from the ATMS. The AMSU-A noise-equivalent differential temperature (NEDT) is 0.25 K for temperature-sounding channels 5–9; 0.4 K for channels 10 and 11; and 0.6, 0.8, and 1.2 K for channels 12, 13, and 14, respectively. The NEDTs for the corresponding ATMS channels are equal to or slightly larger than twice those of the AMSU-A NEDTs. More details about the similarities and differences in ATMS and AMSU-A instrument and channel characteristics are given by Mo (1996) and Weng et al. (2012).

3. A brief review on temperature profile retrievals

Using satellite microwave observations to retrieve atmospheric temperatures started soon after the *NOAA-15* satellite was launched. Based on the physical consideration that microwave radiances respond linearly to temperature and that the AMSU-A and ATMS weighting functions are relatively stable, the atmospheric temperature at a specified

pressure level $T(p)$ is expressed as a weighted linear combination of brightness temperature observations at different AMSU-A channels $T_b^{obs}(i)$, where i is the channel number; that is,

$$T(p) = C_0 + \sum_{i=i_{1,p}}^{i_{2,p}} C_i(p) T_b^{obs}(i), \tag{1}$$

where p is the atmospheric pressure. The summation $\sum_{i=i_{1,p}}^{i_{2,p}}$ represents a weighted average of the brightness temperature observations of a subset of AMSU-A channels 5–14 with channel numbers $(i_{1,p}, i_{1,p}+1, i_{1,p}+2, \ldots, i_{2,p})$ that are selected for obtaining the atmospheric temperature at the pressure level p. The coefficients $C_j(p)$ $(j = 0, i_{1,p}, i_{1,p}+1, i_{1,p}+2, \ldots, i_{2,p})$ are regression coefficients whose values are determined by a least squares fit to some known reference temperatures. Kidder et al. (2000) used radiosonde observations to estimate the regression coefficients. All AMSU-A observations were first adjusted to nadir in order to have a sufficiently large sample of collocated radiosonde and AMSU-A data. Kidder et al. (2000) argued that this needs to be done to reduce scan-angle-dependent biases in the temperature retrieval product caused by varying sample sizes at different scan angles. Channels 1–7 are not used for retrievals above 100 hPa to ensure that there is neither high-terrain contamination nor cloud contamination by heavy precipitation. Channels 1–5 are not used for retrievals from 700 to 115 hPa in order to reduce the contamination from heavy precipitation.

Zhu et al. (2002) modified Eq. (1) to the following form:

$$T(p) = C_0(p) + \sum_{i=3}^{11} C_i(p) T_b^{obs}(i) + C_\theta(p) \frac{1}{\cos\theta}, \quad (2)$$

where θ is the scan angle. The regression coefficients were estimated for each scan angle separately based on radiosonde observations. An additional scan-angle term [i.e., the last term in Eq. (2)] was added.

Tian and Zou (2016) found that the last term in Eq. (2) does not completely remove scan-angle-dependent biases from the temperature retrieval product. They thus proposed two modifications. First, the retrieval equation is modified as follows:

$$T(p) = C_0(p,\theta) + \sum_{i=i_{1,p}}^{i_{2,p}} C_i(p,\theta) T_b^{obs}(i), \quad (3)$$

where only those channels that are highly correlated to the temperature at the p level are selected for the retrieval of $T(p)$. Second, the regression coefficients are estimated using ATMS or AMSU-A data and numerical weather prediction (NWP) model fields of temperature over the 2-week period right before the time period the retrieval is to be obtained. In this way, the impacts of scan-angle-dependent and temperature-dependent biases on the temperature retrieval product can be effectively removed. This method is used for obtaining the warm-core structure of Hurricanes Harvey, Irma, and Maria.

The regression described above employs global data from 55°S to 55°N during the 2-week period prior to a targeted TC case. This means that the regression coefficients in Eq. (3) would have to be obtained for every storm. A more explicit latitudinal-dependent regression algorithm is likely needed for those TCs whose lifespans cross a large latitudinal range. Examples are those TCs that initiate in the deep tropics, develop and intensify in the subtropics while moving northwestward, and recurve to move northeastward in the midlatitudes. In this case, a training period longer than 2 weeks would be required so that a sufficient number of data samples could be compiled for obtaining the regression coefficients in different latitudinal bands. Further investigations will be carried out in a follow-on study to examine the sensitivity of the warm-core retrieval.

4. Characteristics of Hurricane Irma

a. Case description

Irma was an Atlantic hurricane that originated at low latitudes in the deep tropics on 30 August 2017, exited
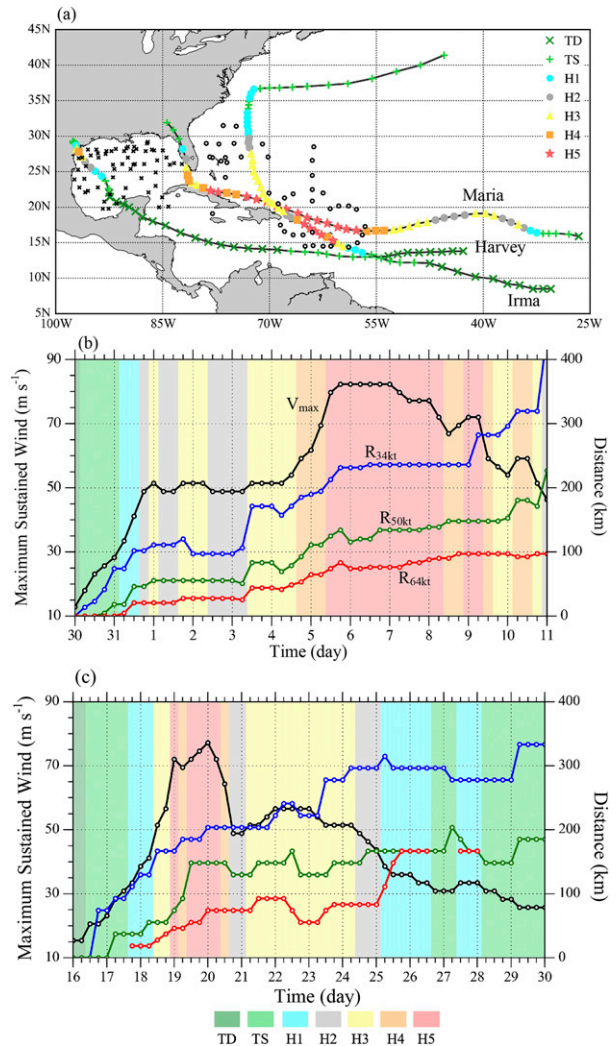

FIG. 1. (a) The best track of Hurricane Irma from 0000 UTC 30 Aug to 0000 UTC 12 Sep, Hurricane Harvey from 1200 UTC 13 Aug to 1800 UTC 31 Aug, and Hurricane Maria from 0000 UTC 14 Sep to 0000 UTC 30 Sep 2017. (b) The temporal evolution of the maximum sustained wind V_{max} (black curve), the radii of 34- (blue curve), 50- (green curve), and 64-kt (red curve) winds, and intensity category (color shading; legend at bottom) from 0000 UTC 30 Aug to 0000 UTC 11 Sep 2017. Also shown in (a) are the dropsonde locations that were collocated with ATMS observations gathered in Irma (42 profiles) from 4 to 10 Sep and gathered in Harvey (76 profiles) from 18 Aug to 3 Sep. The collocation criteria are defined as no more than a 3-h time difference and a 100-km spatial separation. (c) As in (b), but for Hurricane Maria from 0000 UTC 16 Sep to 0000 UTC 30 Sep 2017. TD, TS, and H1–H5 stand for tropical depression, tropical storm, and hurricane categories 1–5.

the coast of West Africa, and passed over or near the Cape Verde Islands (Fig. 1a). Irma rapidly intensified shortly after its formation to become a category-2 hurricane at 1800 UTC 31 August 2017 and a category-3 hurricane at 0000 UTC 1 September 2017 (Fig. 1b). The intensity of Irma fluctuated between categories 2 and 3

from 1800 UTC 31 August to 1800 UTC 4 September 2017 because of a series of eyewall replacement cycles and reached category 5 at 1200 UTC 5 September 2017. At this time, the peak intensity reached a sustained wind speed of $81.9\,\mathrm{m\,s^{-1}}$ ($295\,\mathrm{km\,h^{-1}}$) and a minimum pressure of 914 hPa. Irma made its first landfall in Cuba as a category-5 hurricane on 9 September 2017, a second landfall in Cudjoe Key, Florida, as a category-4 hurricane with maximum sustained winds of $59.7\,\mathrm{m\,s^{-1}}$ ($215\,\mathrm{km\,h^{-1}}$), and a third landfall on Marco Island, Florida, as a category-3 hurricane on 11 September 2017. Note that these intensity values were derived from the working best track of Irma and are preliminary and subject to further refinement.

Irma had the strongest maximum sustained winds since Hurricane Wilma in 2005. It was the most intense hurricane to strike the United States since Katrina in 2005 and the second major hurricane of the 2017 Atlantic hurricane season. Irma developed into one of the most intense storms of the season in the Atlantic as it moved over the warm, open ocean for a long distance without encountering land. Other factors influencing the hurricane intensity such as water temperature; depth of the warm water; diabatic and adiabatic warming associated with entrainment and detrainment of convective bursts, respectively; and the strength of the shear need to be examined in order to understand why Irma reached category-5 status. Since Irma had a long lifetime and made three landfalls, it caused widespread and catastrophic property damage and many deaths in Barbuda, Saint Barthélemy, Saint Martin, Anguilla, and the Virgin Islands as a category-5 hurricane.

b. Validation of ATMS-retrieved temperatures with dropsonde data

Dropsondes are critical observational instruments often used by NOAA hurricane reconnaissance aircraft to obtain vertical profiles of temperature, wind speed and direction, humidity, and pressure from the altitude of the aircraft to the surface. To gather data on Irma, dropsondes were deployed under heavy rain and wind conditions after 3 September 2017. Figure 1a shows the locations of 118 dropsonde profiles that were collocated with ATMS observations. The collocation criteria are defined as no more than a 3-h time difference and a 100-km spatial separation. Out of the 118 dropsondes, 42 profiles were gathered in Irma from 4 to 10 September 2017 and 76 profiles were gathered in Hurricane Harvey from 18 August to 3 September 2017. Figure 2a gives the data count of dropsonde profiles with respect to the radial distance from the centers of Hurricanes Irma and Harvey. There is only one dropsonde profile within 200 km of the hurricane centers but more than 13 and 17

profiles within 200–300 and 300–400 km of the hurricane centers, respectively. A spaghetti map of the temperature differences between ATMS retrievals and the 118 collocated dropsonde profiles is provided in Fig. 2b along with the mean difference profile and root-mean-square errors (RMSEs). Most dropsondes were released from an altitude of ~180 hPa except for 24 dropsondes that were released from higher altitudes in Irma. Mean differences between the ATMS temperature retrievals and the dropsonde temperatures are within $\pm0.7\,\mathrm{K}$ in the vertical layer between 180 and 750 hPa, which well covers the warm-core depth of Hurricane Irma from 30 August to 11 September 2017 (Fig. 2b). The RMSEs within this layer are ~1 K. Theoretically speaking, the strong attenuation of brightness temperatures in the lower channels in the TC eyewall greatly degrades the temperature retrieval accuracies in this region. The fact that the differences between dropsonde-observed and ATMS-retrieved vertical temperature profiles near the hurricane center are of similar magnitudes as those farther away from the center is due to the coarse horizontal resolutions of ATMS observations (~40 and ~140 km at the centers and edges of ATMS swaths, respectively). Also, the TC eye diameter can be significantly smaller than the ATMS and AMSU-A sounding channels' resolutions, which results in an undersampling of TC warm-core anomalies near TC centers. In some cases, the vertical resolutions of the microwave sounders cannot resolve details about the TC warm-core vertical structure.

c. Warm-core structures of Hurricanes Irma and Harvey

The temporal evolution of the vertical variations in ATMS-retrieved temperature anomalies at Irma's center from 30 August to 11 September 2017 is shown in Fig. 2c. The temperature anomaly is defined as the deviation from the mean environmental temperature within a 15° latitude–longitude geographic box centered on the storm but outside of the 34-kt-wind radii (1 kt = $0.51\,\mathrm{m\,s^{-1}}$) and with storm perturbations excluded. The ATMS-retrieved warm core of Irma was located at ~250 hPa. This altitude is consistent with the altitude of the secondary weaker maximum temperature anomaly found by Stern and Nolan (2012) from ideal numerical experiments and the upper-level warm core that was formed from an adiabatic warming of the subsidence of stratospheric air associated with the detrainment of convective bursts in a real-case numerical simulation done by Chen and Zhang (2013). As Irma intensified with time, the temperature anomaly and the warm-core depth also increased. The upper boundary of the warm core rose more steadily than the bottom boundary
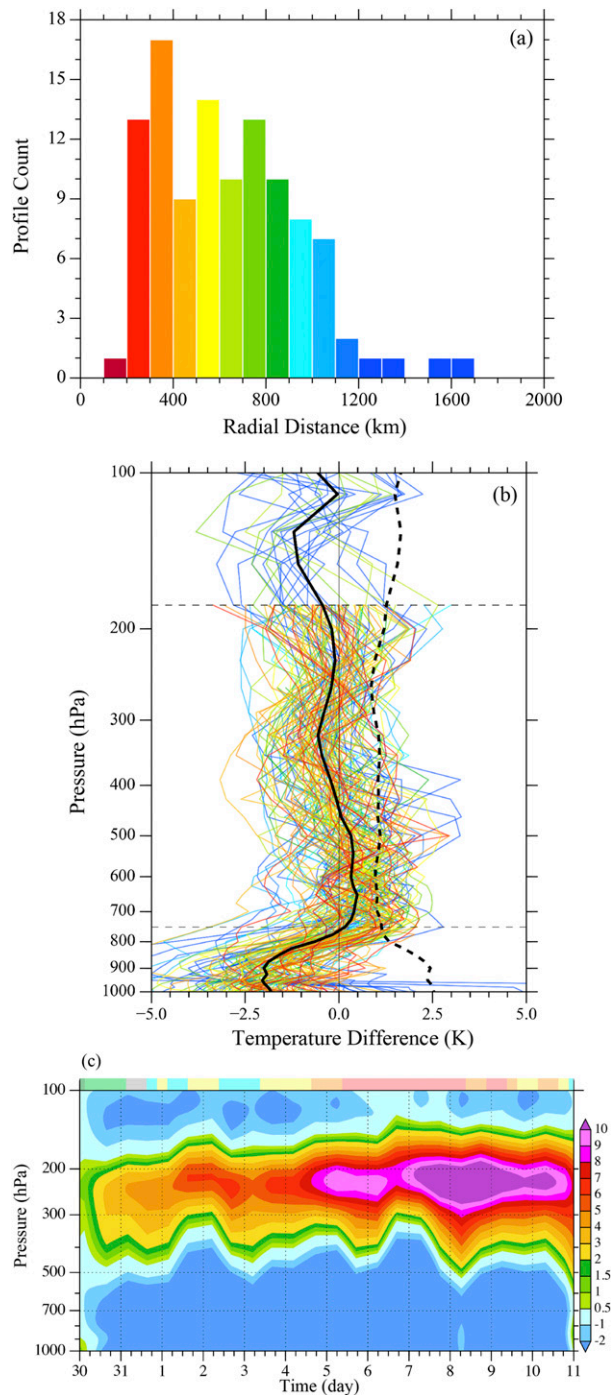
FIG. 2. (a) Number of dropsonde profiles as a function of the radial distance from the centers of Hurricanes Irma and Harvey, and (b) spaghetti map (thin colored curves), mean values (thick solid black line), and RMSEs (black dashed line) of the vertical profiles of temperature differences between ATMS retrievals and collocated dropsonde measurements. The total number of collocated dropsonde profiles is 118 and 24 below and above 180 hPa, respectively. The color convention of the curves in (b) is as in (a), representing the radial distances of the dropsonde profiles from the center of Hurricanes Irma and Harvey. (c) Temporal evolution of

because of the more active and stronger diabatic activity at lower levels. It is important to mention that throughout the life cycles of TCs such as Hurricane Irma, the actual warm cores of TCs can have significant vertical structure differences throughout the troposphere. The fact that little change occurred at the lower levels of Irma's warm core could be due to the inability of the microwave sounder to adequately resolve temperatures in its observational channels.

Figure 3 shows the horizontal distributions of the ATMS-derived warm-core structure at 250 hPa with (Fig. 3a) and without (Fig. 3b) random noise mitigation, and Visible Infrared Imaging Radiometer Suite (VIIRS) day–night band (DNB) radiance observations (Fig. 3c) at 0536 UTC 6 September 2017. Also shown are vertical cross sections of the ATMS-derived temperature warm-core anomaly and liquid water path (LWP; Weng et al. 2003) along the west–east (Fig. 3d) and south–north (Fig. 3e) directions at the same time and passing through Irma's center. The maximum warm-core temperature anomaly was warmer than 10 K. Figure 4 gives another example showing the horizontal distribution of the ATMS-derived temperature warm-core structure at 250 hPa (Fig. 4a), VIIRS DNB radiance observations (Fig. 4b), the vertical cross section of the ATMS-derived temperature warm-core anomaly and LWP variations through Hurricane Harvey's center along the west–east direction (Fig. 4c), and the horizontal distribution of the VIIRS cloud-top pressure (Fig. 4d) at 0600 UTC 25 August 2017. A spiral rainband–like band of warm temperature anomalies greater than 2 K was located to the southeast of the warm-core center at 250 hPa (Fig. 3a), which matches geographically with the spiral cloud distribution of the VIIRS DNB radiance observations (Fig. 3c) available at the same time. Such a spiral rainband–like warm temperature anomaly feature is not readily seen in the warm-core retrieval when ATMS random noise is not removed before the retrieval (Fig. 3b). A spiral rainband–like warm anomaly appears to the northeast of the main warm-core center of Hurricane Harvey (Fig. 4a), which also coincides with the spiral cloud distribution seen in VIIRS DNB radiance observations that show high cloud-top altitudes (Figs. 4c,d). The banded features of warm anomalies are possibly not real and may result from rain contamination in low-tropospheric channels 5 and 6. The vertical cross

←

the vertical variations in ATMS-retrieved temperature anomalies at Irma's center from 30 Aug to 11 Sep 2017. The color convention for the intensity of Hurricane Irma shown along the top of (c) is the same as that shown at the bottom of Fig. 1c.
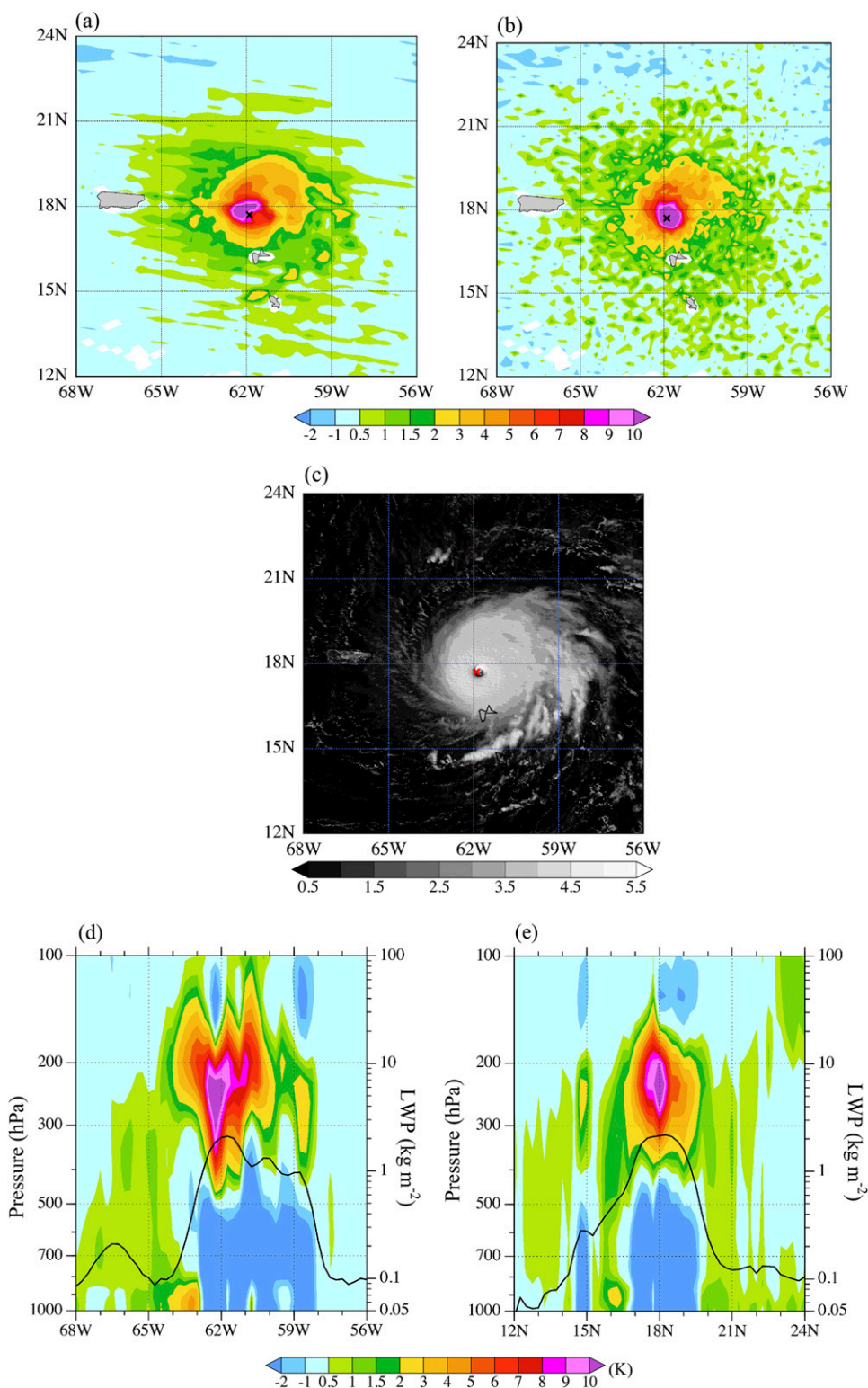
FIG. 3. Horizontal distributions of the ATMS-derived temperature warm-core structure at 250 hPa (a) with and (b) without random noise mitigation (K) and (c) VIIRS DNB radiance observations. The red cross in (c) shows the location of center of Hurricane Irma. Vertical cross sections of the ATMS-derived temperature warm-core anomaly (color shaded) and LWP (black curve) through Irma's center along the (d) west–east and (e) south–north directions at 0536 UTC 6 Sep 2017.
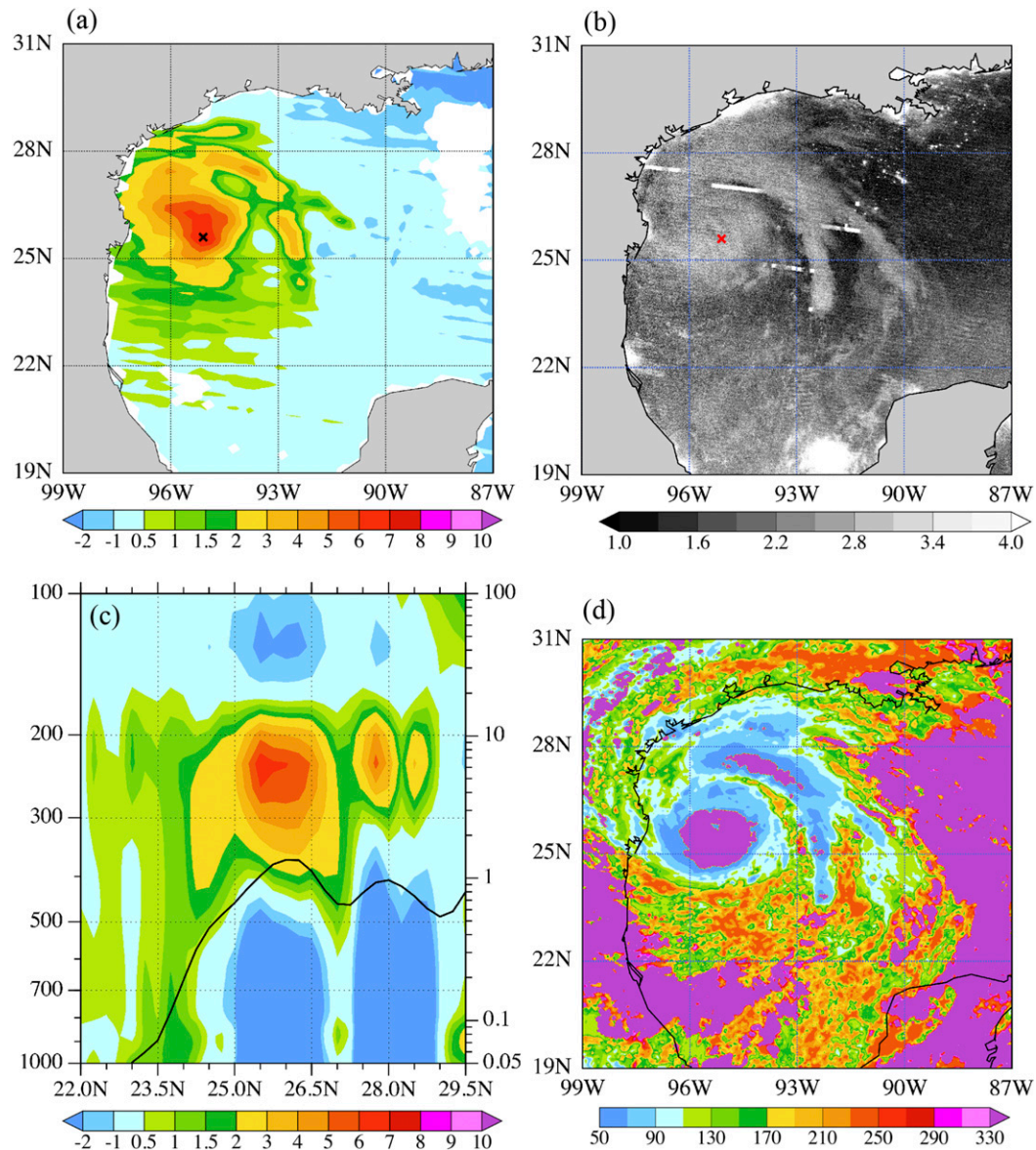
FIG. 4. (a) Horizontal distribution of the ATMS-derived temperature warm-core structure at 250 hPa (K), (b) VIIRS DNB radiance observations, where the red cross shows the location of the center of Hurricane Harvey, (c) vertical cross section of the ATMS-derived temperature warm-core anomaly (color shaded; K) and LWP (black curve; kg m^{-2}) through Hurricane Harvey's center along the west–east direction, and (d) the horizontal distribution of VIIRS cloud-top pressure (hPa) at 0600 UTC 25 Aug 2017.

section of the ATMS-derived temperature warm-core anomaly along the west–east direction (Fig. 3d) is less symmetric than that along the south–north direction (Fig. 3e) owing to rainband structures that are located to the south of the warm-core center. Note that the altitude variation along the lower boundary of the warm core has an antiphase variation to that of the LWP along the west–east direction (Figs. 3d and 4c). This is consistent with the finding by Willoughby (1998) who reported that convection in the eyewall causes the warming by doing

work on the eye to force the thermally indirect subsidence. The cold anomalies in the lower troposphere, however, are likely due to some attenuation by precipitation of low-tropospheric channel-5 and -6 radiances near the storm center.

It is further shown that the temporal evolution of the maximum temperature warm-core anomalies at 250 hPa derived from the *SNPP* ATMS and the AMSU-A on board the *NOAA-15*, *-18*, and *-19* satellites follows the minimum sea level pressure (MSLP; Fig. 5a) more

closely than the maximum sustained wind (Fig. 5b). This is expected because the temperature anomaly is more correlated with the pressure anomaly through the hydrostatic relationship, while the maximum sustained winds could deviate from the observed pressure and temperature anomalies as a result of small-scale features not well resolved by the sounders or dynamic sources not observed by the sounders at all. The maximum warm-core anomalies retrieved from the afternoon orbits of the *SNPP* and *NOAA-19* satellites (LECTs are 1330 and 1530 LT, respectively) are consistently larger than those from the early morning orbits of the *NOAA-15* and *NOAA-18* satellites (LECTs are 0621 and 0715 LT, respectively), reflecting the diurnal variations in warm cores.

In addition to capturing the intensity changes of Hurricane Irma, the ATMS- and AMSU-A-derived warm cores also capture the size variations of Hurricane Irma. Figure 6 shows the temporal evolution of the radial variation in ATMS-retrieved temperature warm-core anomalies at 250 hPa within a 500-km radial distance along the west–east direction through the center of Hurricane Irma. Also plotted in Fig. 6 are the radii of warm cores with temperature anomalies greater than 2, 4, 6, and 8 K from 30 August to 11 September 2017. Compared with the 34-, 50-, and 64-kt-wind radii shown in Fig. 1b, the sizes of the warm cores in the upper troposphere at a set of fixed temperature anomalies retrieved from ATMS temperature-sounding channels are good indicators of the hurricane size near the surface. Similar results relating AMSU-derived temperature distributions to TC size parameters were reported by others (Knaff et al. 2004; Bessho et al. 2006; Demuth et al. 2006; Oyama 2014).

5. Diurnal variations in the warm-core structures of Hurricane Maria

The finding that Irma's warm-core retrievals from different polar-orbiting satellites with varying LECTs reflect a diurnal variation in the maximum warm-core intensity is further substantiated by the case of Hurricane Maria. Hurricane Maria is chosen for this illustration because during its lifespan, *MetOp-B* AMSU-A observations were available. Hurricane Maria was the second category-5 hurricane of the hyperactive Atlantic hurricane season of 2017. It was a major hurricane that threatened the Leeward Islands 2 weeks after the passage of Hurricane Irma (see Fig. 1a). The best track of Hurricane Maria from 0000 UTC 14 September to 0000 UTC 30 September is shown in Fig. 1a. The temporal evolutions of the maximum sustained wind, and the radii of 34-, 50-, and 64-kt winds from 0000 UTC 16 September to
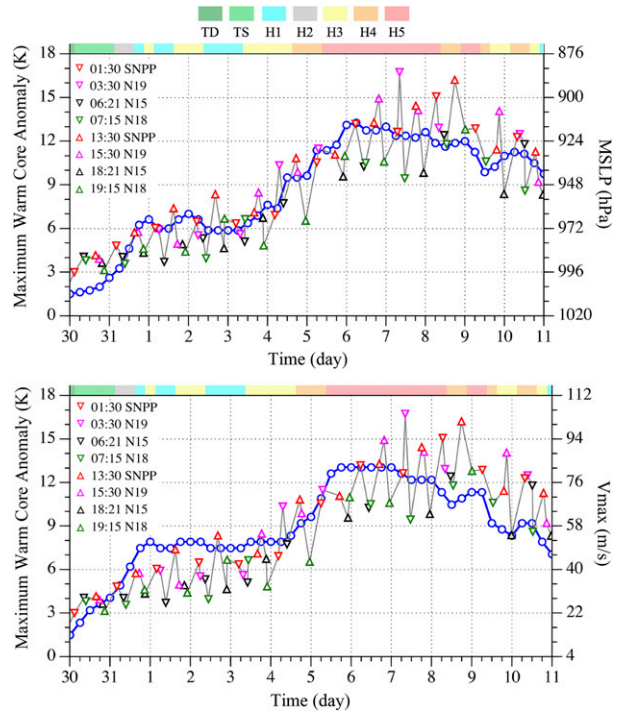

FIG. 5. Temporal evolutions of (a) the ATMS- and AMSU-A-derived temperature warm-core anomalies at 250 hPa (gray curve with triangles) and the best track MSLP (blue curve with blue open circles) and (b) the ATMS- and AMSU-A-derived maximum temperature warm-core anomalies (colored triangles connected by the gray line) and the best track maximum sustained wind (blue curve with blue open circles) at the descending (downward triangle) and ascending (upward triangle) nodes of the *SNPP* (green), *NOAA-15* (black), *NOAA-18* (blue), and *NOAA-19* (red) satellites from 30 Aug to 11 Sep 2017. Local equator crossing times are given for each node. The color convention for the intensity of Hurricane Irma is shown above (a). TD, TS, and H1–H5 stand for tropical depression, tropical storm, and hurricane categories 1–5.

0000 UTC 30 September is shown in Fig. 1c. Maria intensified rapidly from 18 to 20 September before approaching the Leeward Islands and reached category-5 status during 19–20 September. It remained a category-3 hurricane as it moved away from the islands over the next 4 days (21–24 September). After this period, it started to weaken. The best track of Maria experienced a sharp recurve on 28 September, changing direction from north to east where Maria became a tropical storm in the midlatitudes (Fig. 1a).

Figure 7 shows the temporal evolutions of the ATMS- and AMSU-A-derived maximum temperature warm-core anomalies and the best track MSLP (Fig. 7a), and the best track maximum sustained winds (Fig. 7b) at the descending and ascending nodes of the *SNPP*, *NOAA-15*, *NOAA-18*, *NOAA-19*, and *MetOp-B* satellites from 0000 UTC 16 September to 0000 UTC 30 September. The satellite microwave sounders involved in Fig. 7 for
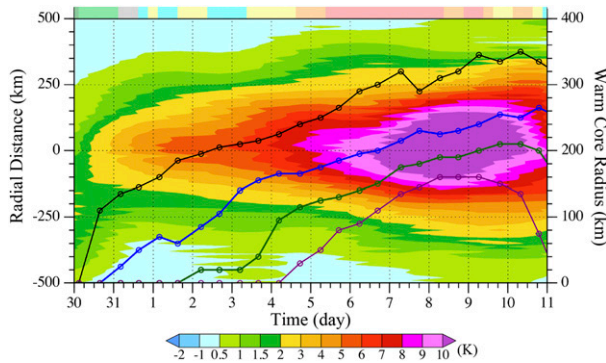
FIG. 6. The temporal evolution of the radial variation in ATMS-retrieved temperature warm-core anomalies at 250 hPa within a 500-km radial distance along the west–east direction through the center of Hurricane Irma, and the radii of warm cores with temperature anomalies greater than 2 (black curve), 4 (blue curve), 6 (green curve), and 8 K (purple curve) from 30 Aug to 11 Sep 2017. The color convention for the intensity of Hurricane Irma shown along the top is the same as that shown at the bottom of Fig. 1c. The ATMS observing times are shown by open circles along the four curves.
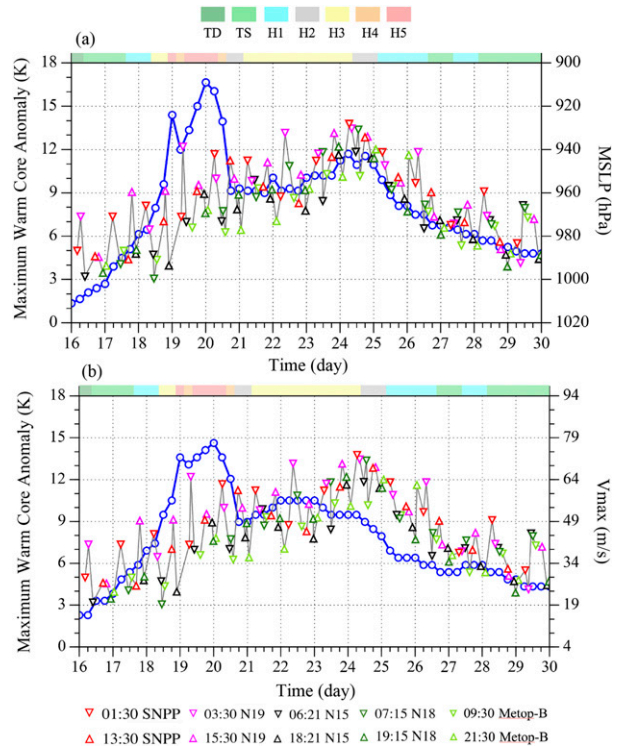

FIG. 7. Temporal evolutions of (a) the ATMS- and AMSU-A-derived maximum temperature warm-core anomalies (gray curve with triangles) and the best track MSLP (blue curve with blue open circles) and (b) the ATMS- and AMSU-A-derived maximum temperature warm-core anomalies (colored triangles connected by the gray line) and the best track maximum sustained wind V_{max} (blue curve with blue open circles) at the descending (downward triangles) and ascending (upward triangles) nodes of the $SNPP$ (green), $NOAA$-15 (black), $NOAA$-18 (blue), $NOAA$-19 (red), and $MetOp$-B (light green) satellites from 16 to 30 Sep 2017. Local equator crossing times are given for each node below (b). The color convention for the intensity of Hurricane Maria is shown above (a). TD, TS, and H1–H5 stand for tropical depression, tropical storm, and hurricane categories 1–5.

Hurricane Maria are the same as those in Fig. 5 for Hurricane Irma except that $MetOp$-B AMSU-A retrievals are added to Fig. 7. As was the case for Irma, the temporal evolution of the maximum temperature warm-core anomalies at 250 hPa derived from the $SNPP$ ATMS and the AMSU-A on board the $NOAA$-15, $NOAA$-18, $NOAA$-19, and $MetOp$-B satellites followed the MSLP (Fig. 7a) quite closely except during the period when Maria underwent a rapid intensification (18–20 September). The temporal evolution of the maximum temperature warm-core anomalies at 250 hPa followed less closely the maximum sustained winds (Fig. 7b). The fact that the upper-level warm-core intensity did not increase as rapidly as the MSLP or maximum sustained winds from 18 to 20 September suggests that the rapid intensification had to do with the low-level troposphere. Because of a strong attenuation of the brightness temperatures for the lower-level sounding channels in the TC eyewall, the temperature retrieval skill was greatly diminished in this region.

An example showing the warm-core structural changes at multiple times on a single day is provided in Fig. 8. We first point out that the eastern half of the warm core is successfully retrieved even though it was located near the edge of the $NOAA$-18 AMSU-A swath. The temperature anomalies at 250 hPa retrieved from $MetOp$-B, $NOAA$-15, $NOAA$-18, and $NOAA$-19 microwave temperature-sounding observations as well as $SNPP$ ATMS observations on 23 September reveal not only a structural variation but also a diurnal intensity variation in Hurricane Maria. To substantiate this

observation of a diurnal variation in the warm-core intensity in the upper troposphere, Fig. 9 shows the diurnal variations in the maximum temperature anomalies at 250 hPa of Hurricane Maria over the 10-day period of 17–26 September 2017. The upper-level warm cores are stronger at night than in the day (Fig. 9b) when Maria evolved from a tropical depression on 16 September to a category-5 hurricane on 19 September, then weakened to a category-2 hurricane on 20 September, only to strengthen again and stabilize as a category-3 hurricane from 25 to 26 September. Since the warm-core temperature anomalies are obtained by subtracting environmental temperatures from AMSU-A/ATMS-retrieved temperatures, we also examined environmental-mean temperatures at 250 hPa for Hurricane Maria during this 10-day period (Fig. 9c). The environmental-mean
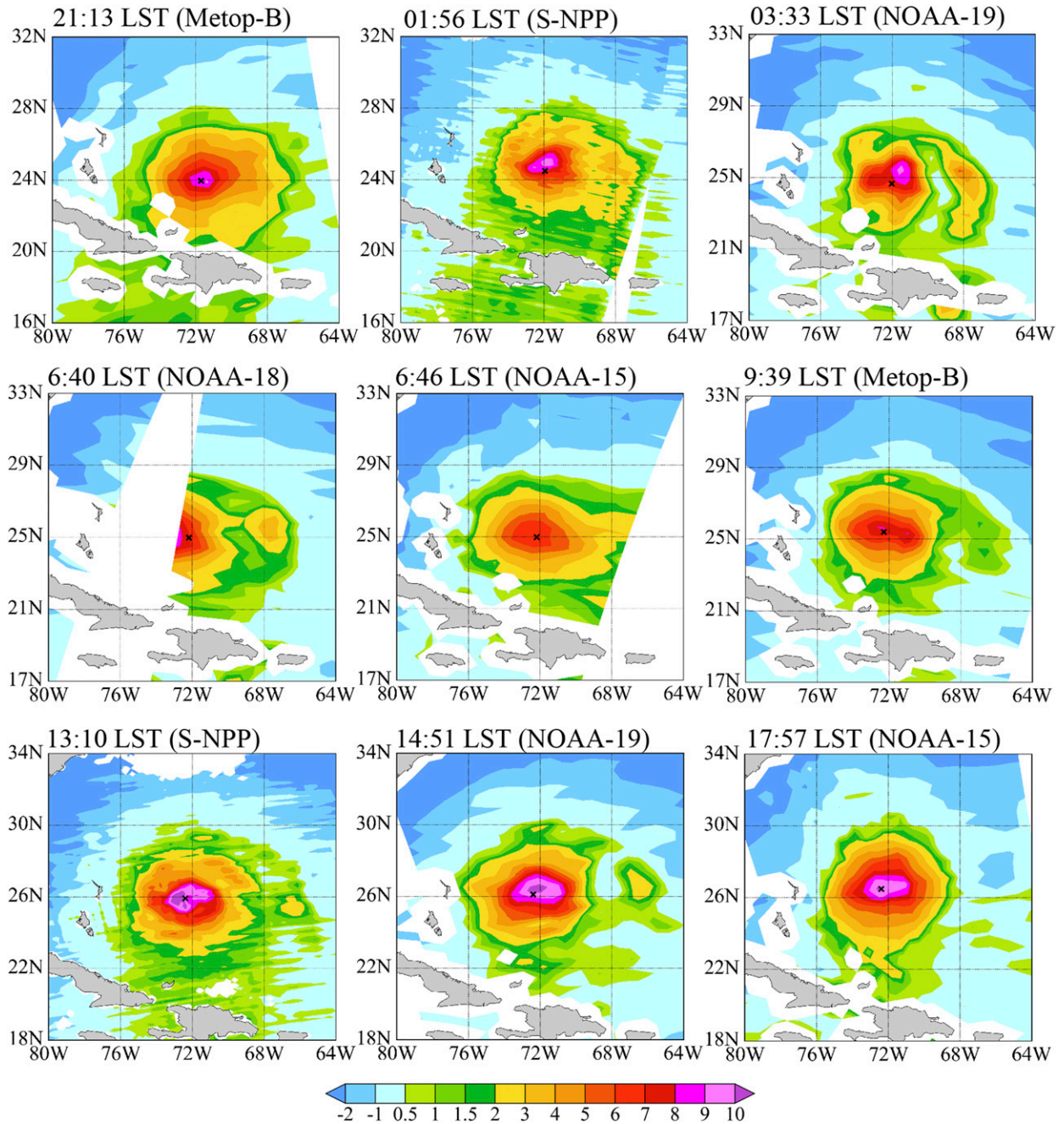
FIG. 8. Hurricane Maria's warm-core temperature anomaly structures at 250 hPa (K) on 23 Sep 2017 retrieved from *MetOp-B* and *NOAA-15*, *-18*, and *-19* AMSU-A observations as well as *SNPP* ATMS observations. The LST and satellite names are given above each panel.

temperatures are slightly lower at midnight but by no more than 0.2 K below the daily average. The warm-core anomalies at night are more than 2 K greater than the 1-day average. Note that as Hurricane Maria moved from lower to higher latitudes and intensified (see Fig. 1), overall, both the environmental temperatures and warm-core temperature anomalies increased. The

inner-core temperatures (Fig. 9b) increased more than the environmental temperatures (Fig. 9c). Figure 10 shows the 500-km-radii mean brightness temperatures at 10.7 μm observed by *Geostationary Operational Environmental Satellite-13* (*GOES-13*) centered on Hurricanes Irma (Fig. 10a) and Maria (Fig. 10b). As reported by Dunion et al. (2014), the period between the
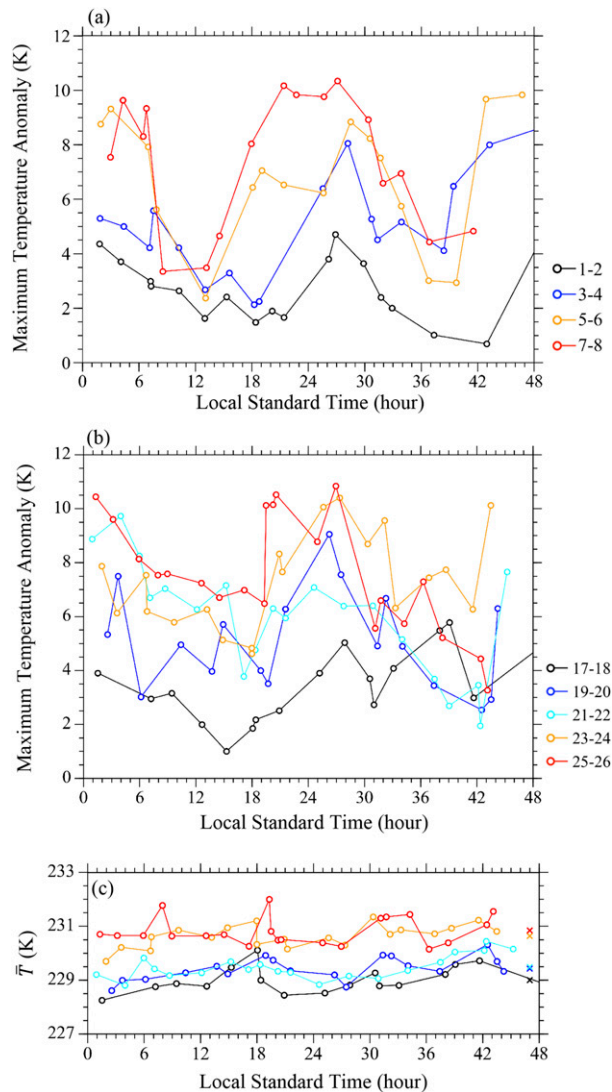
FIG. 9. Diurnal variations in the maximum temperature anomaly at 250 hPa for (a) Hurricane Irma on 1–2 (black), 3–4 (blue), 5–6 (orange), and 7–8 (red) Sep 2017; and for (b) Hurricane Maria on 17–18 (black), 19–20 (blue), 21–22 (cyan), 23–24 (orange), and 25–26 (red) Sep 2017. (c) Environmental temperatures at 250 hPa for Hurricane Maria.

local sunset and the next sunrise is the optimal time for stronger inner-core convection to occur and for relatively colder brightness temperatures to be seen. Peak convection is generally in phase with the diurnal variation of the warm cores shown in Fig. 9 although it is not exactly aligned. The reason for this discrepancy requires further study. The argument by Willoughby (1998) on convection in the eyewall forcing subsidence (warming) could be one explanation for the phasing misalignment. Our results concerning the diurnal cycle of inner-core warm temperature anomalies are consistent with the finding reported by Leppert and Cecil (2016). Using passive and active microwave measurements from the
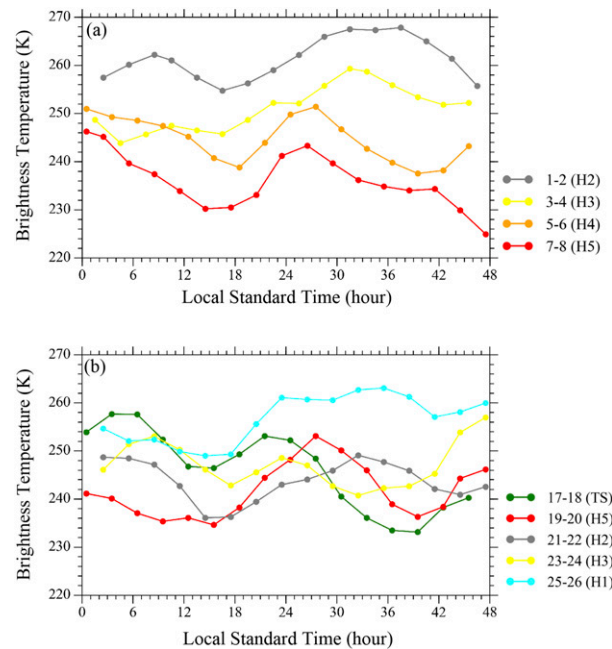

FIG. 10. *GOES-13*-based 3-hourly 500-km-radii mean brightness temperatures at 10.7 μm (a) from 1 to 8 Sep following Hurricane Irma and (b) from 17 to 26 Sep following Hurricane Maria. TS and H1–H5 (in parentheses) stand for tropical storm and hurricane categories 1–5.

Tropical Rainfall Measuring Mission Microwave Imager and Precipitation Radar, Leppert and Cecil (2016) found that the TC inner core is associated with a single-peaked diurnal cycle at upper levels (8–10 km) with a maximum at 2230–0430 local standard time (LST).

A spiral rainband–like warm temperature anomaly, which is seen in Figs. 3 and 4 for Hurricanes Irma and Harvey, respectively, is also seen for Maria at 0830, 1100, and 1430 UTC 23 September 2017 based on AMSU-A observations from the *NOAA-19*, *NOAA-18*, and *MetOp-B* satellites, respectively. Figure 11 shows *GOES-13* brightness temperature observations at 10.7 μm at these times on that day. The spiral rainband-like warm temperature anomalies seen in Fig. 8 at 0830, 1100, and 1430 UTC derived from *NOAA-19*, *NOAA-18*, and *MetOp-B* AMSU-A retrievals correspond geographically to the spiral cloud band seen from *GOES-13* (i.e., the areas with very low brightness temperatures). As mentioned before, the rainband structures of the warm core could be caused by attenuation associated with scattering from heavy convection for the low-level sounding channels (e.g., channels 5 and 6). Further investigation is needed and plans for a follow-on study are under way.

6. Summary and conclusions

A series of strong hurricane activities occurred over the Atlantic Ocean from near the end of August to the
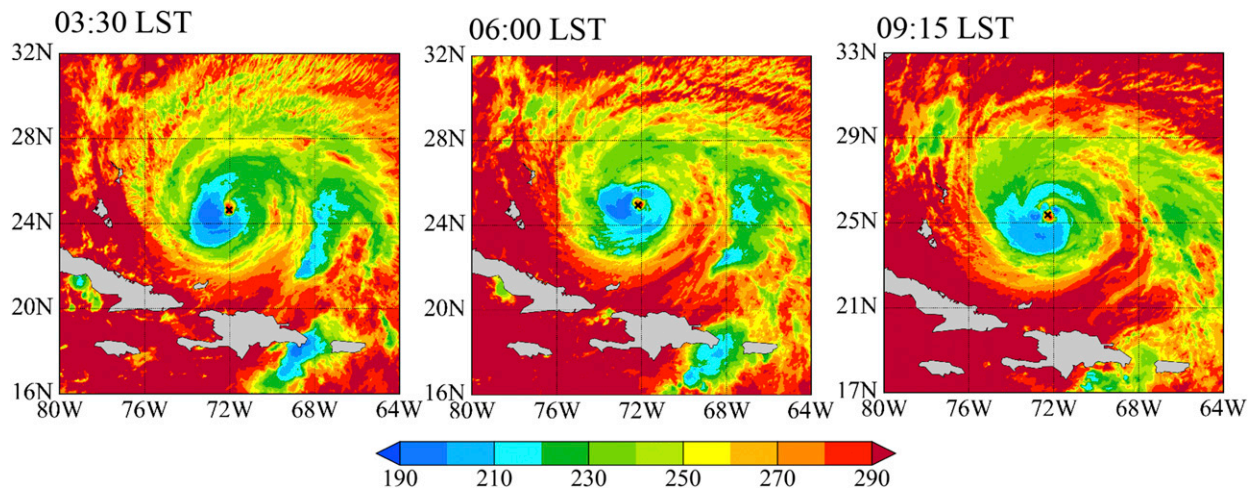
FIG. 11. *GOES-13* brightness temperature observations at 10.7 μm (K) at 0330, 0600, and 0915 LST, corresponding to the observing times of the AMSU-A on board the *NOAA-19*, *NOAA-18*, and *MetOp-B* satellites on 23 Sep 2017.

beginning of October 2017. Currently, there are four NOAA polar-orbiting operational environmental satellites and two EUMETSAT satellites carrying microwave temperature-sounding instruments that provide global microwave observations several times daily. They are the ATMS on board the *SNPP* satellite and the AMSU-A on board the *NOAA-15*, *NOAA-18*, *NOAA-19*, *MetOp-A*, and *MetOp-B* satellites. This study demonstrates that these polar-orbiting operational satellite microwave radiometers captured the size and intensity changes of Hurricanes Irma, Harvey, and Maria in 2017. The atmospheric temperatures retrieved from ATMS and AMSU-A temperature-sounding channels provide a four-dimensional view of hurricane warm-core structures, the temporal evolution of sizes consistent with the 34-, 50-, and 64-kt-wind radii near the surface, and the diurnal variation of the inner-core temperature anomaly.

The temporal resolutions of the four currently available NOAA polar-orbiting microwave sounders are still not high enough to fully capture fast-evolving processes that occur within hurricanes. A future small satellite (smallsat) constellation with each smallsat carrying a microwave sensor on board would allow these fast-evolving processes to be fully monitored and predicted ([Ma et al. 2017](#)). An example of this is the Time-Resolved Observations of Precipitation structure and storm Intensity with a Constellation of Smallsats mission (TROPICS; https://tropics.ll.mit.edu/CMS/tropics/). The TROPICS mission consists of 12 CubeSats carrying 12-channel microwave radiometers that include 7 channels near the 118.75-GHz oxygen absorption line, which can provide atmospheric temperature measurements. Until the CubeSats are finally launched, information from current operational environmental satellites can be used to capture some of the eyewall replacement processes.

REFERENCES

Bessho, K., M. DeMaria, and J. A. Knaff, 2006: Tropical cyclone wind retrievals from the Advanced Microwave Sounding Unit: Application to surface wind analysis. *J. Appl. Meteor. Climatol.*, **45**, 399–415, https://doi.org/10.1175/JAM2352.1.

Brueske, K. F., and C. S. Velden, 2003: Satellite-based tropical cyclone intensity estimation using the NOAA-KLM series Advanced Microwave Sounding Unit (AMSU). *Mon. Wea. Rev.*, **131**, 687–697, https://doi.org/10.1175/1520-0493(2003)131<0687:SBTCIE>2.0.CO;2.

Chen, H., and D.-L. Zhang, 2013: On the rapid intensification of Hurricane Wilma (2005). Part II: Convective bursts and the upper-level warm core. *J. Atmos. Sci.*, **70**, 146–162, https://doi.org/10.1175/JAS-D-12-062.1.

Demuth, J. L., M. DeMaria, J. A. Knaff, and T. H. Vonder Haar, 2004: Evaluation of Advanced Microwave Sounding Unit tropical-cyclone intensity and size estimation algorithms. *J. Appl. Meteor.*, **43**, 282–296, https://doi.org/10.1175/1520-0450(2004)043<0282:EOAMSU>2.0.CO;2.

——, ——, and ——, 2006: Improvement of advanced microwave sounding unit tropical cyclone intensity and size estimation algorithms. *J. Appl. Meteor. Climatol.*, **45**, 1573–1581, https://doi.org/10.1175/JAM2429.1.

Dunion, J. P., C. D. Thorncroft, and C. S. Velden, 2014: The tropical cyclone diurnal cycle of mature hurricanes. *Mon. Wea. Rev.*, **142**, 3900–3919, https://doi.org/10.1175/MWR-D-13-00191.1.

Durden, S. L., 2013: Observed tropical cyclone eye thermal anomaly profiles extending above 300 hPa. *Mon. Wea. Rev.*, **141**, 4256–4268, https://doi.org/10.1175/MWR-D-13-00021.1.

Kidder, S. Q., M. D. Goldberg, R. M. Zehr, M. DeMaria, J. F. W. Purdom, C. S. Velden, N. C. Grody, and S. J. Kusselson, 2000: Satellite analysis of tropical cyclones using the Advanced Microwave Sounding Unit (AMSU). *Bull. Amer. Meteor. Soc.*, **81**, 1241–1260, https://doi.org/10.1175/1520-0477(2000)081<1241:SAOTCU>2.3.CO;2.

Knaff, J. A., S. A. Seseske, M. DeMaria, and J. L. Demuth, 2004: On the influences of vertical wind shear on symmetric tropical cyclone structure derived from AMSU. *Mon. Wea. Rev.*, **132**, 2503–2510, https://doi.org/10.1175/1520-0493(2004)132<2503:OTIOVW>2.0.CO;2.

Leppert, K. D., III, and D. J. Cecil, 2016: Tropical cyclone diurnal cycle as observed by TRMM. *Mon. Wea. Rev.*, **144**, 2793–2808, https://doi.org/10.1175/MWR-D-15-0358.1.

Ma, Y., X. Zou, and F. Weng, 2017: Potential applications of small satellite microwave observations for monitoring and predicting global fast-evolving weathers. *IEEE J. Sel. Top. Appl. Earth Obs. Remote Sens.*, **10**, 2441–2451, https://doi.org/10.1109/JSTARS.2017.2663335.

Mo, T., 1996: Prelaunch calibration of the advanced microwave sounding unit-A for NOAA-K. *IEEE Trans. Microwave Theory Tech.*, **44**, 1460–1469, https://doi.org/10.1109/22.536029.

Oyama, R., 2014: Estimation of tropical cyclone central pressure from warm core intensity observed by the Advanced Microwave Sounding Unit-A (AMSU-A). *Pap. Meteor. Geophys.*, **65**, 35–56, https://doi.org/10.2467/mripapers.65.35.

Stern, D. P., and D. S. Nolan, 2012: On the height of the warm core in tropical cyclones. *J. Atmos. Sci.*, **69**, 1657–1680, https://doi.org/10.1175/JAS-D-11-010.1.

Tian, X., and X. Zou, 2016: ATMS- and AMSU-A-derived hurricane warm core structures using a modified retrieval algorithm. *J. Geophys. Res. Atmos.*, **121**, 12 630–12 646, https://doi.org/10.1002/2016JD025042.

Weng, F., L. Zhao, R. R. Ferraro, G. Poe, X. Li, and N. C. Grody, 2003: Advanced Microwave Sounding Unit cloud and precipitation algorithms. *Radio Sci.*, **38**, 8068, https://doi.org/10.1029/2002RS002679.

——, X. Zou, X. Wang, S. Yang, and M. D. Goldberg, 2012: Introduction to Suomi National Polar-Orbiting Partnership advanced technology microwave sounder for numerical weather prediction and tropical cyclone applications. *J. Geophys. Res.*, **117**, D19112, https://doi.org/10.1029/2012JD018144.

Willoughby, H. E., 1998: Tropical cyclone eye thermodynamics. *Mon. Wea. Rev.*, **126**, 3053–3067, https://doi.org/10.1175/1520-0493(1998)126<3053:TCET>2.0.CO;2.

Zhu, T., and F. Weng, 2013: Hurricane Sandy warm-core structure observed from Advanced Technology Microwave Sounder. *Geophys. Res. Lett.*, **40**, 3325–3330, https://doi.org/10.1002/grl.50626.

——, D.-L. Zhang, and F. Weng, 2002: Impact of the Advanced Microwave Sounding Unit measurements on hurricane prediction. *Mon. Wea. Rev.*, **130**, 2416–2432, https://doi.org/10.1175/1520-0493(2002)130<2416:IOTAMS>2.0.CO;2.